NUMERICAL SIMULATION OF COMPRESSIBLE FLOW WITH LOW MACH NUMBER THROUGH OSCILLATING GLOTTIS

Petra Punčochářová, Jiří Fürst

Czech Technical University in Prague, Faculty of Mechanical Engineering, Department of Technical Mathematics, Prague, Czech Republic

Karel Kozel, Jaromír Horáček

Institute of Thermomechanics AS CR, Centre of Energetics, Prague, Czech Republic

ABSTRACT

The work deals with the numerical solution of 2D unsteady compressible viscous flows in a symmetric channel for a low inlet airflow velocity. The unsteadiness of the flow is caused by a prescribed periodic motion of a part of the channel wall with large amplitudes, nearly closing the channel during the oscillations. The flow in the channel can represent a simplified model of airflow coming from the trachea, through the glottal region with periodically vibrating vocal folds to the human vocal tract.

The numerical solution is realized by finite volume method and the explicit predictor-corrector MacCormack scheme with Jameson artificial viscosity using a grid of quadrilateral cells. The moved grid of quadrilateral cells is considered in the form of conservation laws using Arbitrary Lagrangian-Eulerian method.

1. INTRODUCTION

The fluid-structure interaction problems can be met in many technical and others applications. This study presents the numerical solution of the compressible viscous flows in a symmetric channel, which is a model of the glottal spaces in the human vocal tract. In reality, the airflow coming from the lungs causes the vocal folds self-oscillations, and the glottis is completely closing in normal phonation regimes generating acoustic pressure fluctuations. In this study, the changes of the channel cross-section are prescribed; the channel is harmonically opening and nearly closing as a first approximation of reality enabling the investigation of the airflow field in the glottal region.

Numerical results of the unsteady flows in the channel are presented for inlet Mach number $M_\infty \approx 10^{-2}$, Reynolds number $\mathrm{Re} = 5 \times 10^3$ and for frequency of the wall motion 20 Hz and 100 Hz. When the glottis is closing the airflow velocity is becoming much higher in the narrowest part of the airways, where also the viscous forces are important. Therefore for a correct modelling of a real flow in the glottis, the compressible, viscous and unsteady fluid-flow model should be considered.

The authors present the numerical solution and the simulations of the flow field in the channel performed by the especially developed program.

2. MATHEMATICAL MODEL

The 2D system of Navier-Stokes equations in conservative non-dimensional form has been used as mathematical model to describe the unsteady laminar flow of the compressible viscous fluid in a domain (Fürst et al, 2001):

$$\frac{\partial \mathbf{W}}{\partial t} + \frac{\partial \mathbf{F}}{\partial x} + \frac{\partial \mathbf{G}}{\partial y} = \frac{1}{\mathrm{Re}} \left(\frac{\partial \mathbf{R}}{\partial x} + \frac{\partial \mathbf{S}}{\partial y} \right), \quad (1)$$

where $\mathbf{W} = [\rho, \rho u, \rho v, e]^T$ is vector of conservative variables, $\mathbf{F}$ and $\mathbf{G}$ are the vectors of inviscid fluxes, $\mathbf{R}$ and $\mathbf{S}$ are the vectors of viscous fluxes, $\mathrm{Re} = (2h'\rho'_\infty u'_\infty)/\eta'_\infty$ is Reynolds number given by inflow variables marked by infinity subscript (dimensional variables are marked by the prime), ρ denotes the density, u and v are the components of velocity vector and e is total energy per unit volume. The static pressure is expressed by the equation of state:

$$p = (\kappa - 1) \left[e - \frac{1}{2}\rho \left(u^2 + v^2 \right) \right]. \quad (2)$$

3. MATHEMATICAL FORMULATION

The bounded computational domain D for numerical solution of the system (1) is shown in Fig. 1. It is a scale model of the symmetric
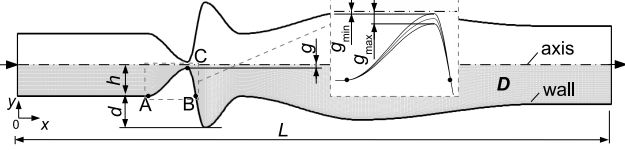
Figure 1: *Domain D, the symmetric channel.*

channel which shape is inspired by a shape of the vocal folds and supraglottal spaces. The computational domain is only the lower half of the symmetric channel. The upper boundary is the axis of symmetry, the lower boundary is the channel wall a part of which, between points A and B, is changing the shape according to a given function of time and axial coordinate:

$$
\begin{aligned}
w(x,t) &= (a_1 + a_t)\left[\sin\left\{\frac{3\pi}{2} + \pi\frac{x - x_A}{x_C - x_A}\right\}\right. \\
&\quad \left. +1\right] + d, \ x \in \langle x_A, \ x_C\rangle, \\
w(x,t) &= 2(a_1 + a_t)\cos\left(\frac{\pi}{2}\frac{x - x_C}{x_B - x_C}\right) + d, \\
&\quad x \in (x_C, \ x_B\rangle, \\
a_t &= a_2\sin(2\pi f t), \ t \in \langle 0, \ 2\pi\rangle, \quad (3)
\end{aligned}
$$

where $f = 5.83 \times 10^{-3}$ is dimensionless frequency, $a_1 = 0.18$, $a_2 = 0.015$. The gap $g = (d + h) - w(x_C, t)$ between the point C and the channel axis is the narrowest part of the channel. The considered dimensions of the domain D are summarized in Table 1.

	x [-]	y [-]	x [mm]	y [mm]
A	1.75	0.4	35	8
B	2.4	0.4	48	8
C	2.3	$w(x_C,t)$	46	$w(x_C,t) \cdot 20$
g_{min}	-	0.01	-	0.2
g_{max}	-	0.07	-	1.4
L	8	-	160	-
h	-	0.4	-	8
d	-	0.4	-	8

Table 1: *Dimensions of the computational domain D.*

The boundary conditions are considered in the following formulation:

1. Upstream conditions: $u_\infty = M_\infty\cos(\alpha)$, $v_\infty = M_\infty\sin(\alpha)$, $\rho_\infty = $ const., p_∞ is extrapolated from domain D and α is angle of incoming flow.

2. Downstream conditions: $p_2 = $ const., $(\rho, \rho u, \rho v)$ are extrapolated from D.

3. Flow on the wall: $(u, v) = (0, v_{wall})$ and $\frac{\partial T}{\partial \vec{n}} = 0$. ($T = p/\rho$ is temperature).

4. Flow on the axis of symmetry: $(u, v) \cdot \vec{n} = 0$.

4. NUMERICAL SOLUTION

The numerical solution uses finite volume method (FVM) in cell centred form on the grid of quadrilateral cells.

The bounded domain D is divided into mutually disjoint sub-domains $D_{i,j}$ (e.g. the quadrilateral cells). The system (1) is integrated over the sub-domains $D_{i,j}$ using Green formula and Mean value theorem. Due to the unsteady domain the integral form of FVM is derived using the Arbitrary Lagrangian-Eulerian (ALE) formulation. ALE method defines homeomorphic mapping of reference domain $D_{t=0}$ at initial time to a domain D_t at $t > 0$ (Honzátko et al, 2006).

The explicit predictor-corrector MacCormack (MC) scheme in the domain with moving grid of quadrilateral cells is used for the numerical solution of the system (1). The scheme is the 2nd order of the accuracy in time and space (Fürst et al, 2001):

$$
\begin{aligned}
\mathbf{W}_{i,j}^{n+1/2} &= \frac{\mu_{i,j}^n}{\mu_{i,j}^{n+1}}\mathbf{W}_{i,j}^n - \frac{\Delta t}{\mu_{i,j}^{n+1}}\sum_{k=1}^{4}\left[\left(\tilde{\mathbf{F}}_k^n\right.\right. \\
&\quad - s_{1k}\mathbf{W}_k^n - \frac{1}{Re}\tilde{\mathbf{R}}_k^n\right)\Delta y_k \\
&\quad - \left(\tilde{\mathbf{G}}_k^n - s_{2k}\mathbf{W}_k^n - \frac{1}{Re}\tilde{\mathbf{S}}_k^n\right)\Delta x_k\Big], \\
\overline{\mathbf{W}}_{i,j}^{n+1} &= \frac{\mu_{i,j}^n}{\mu_{i,j}^{n+1}}\frac{1}{2}\left(\mathbf{W}_{i,j}^n + \mathbf{W}_{i,j}^{n+1/2}\right) \\
&\quad - \frac{\Delta t}{2\mu_{i,j}^{n+1}}\sum_{k=1}^{4}\left[\left(\tilde{\mathbf{F}}_k^{n+1/2} - s_{1k}\mathbf{W}_k^{n+1/2}\right.\right. \\
&\quad - \frac{1}{Re}\tilde{\mathbf{R}}_k^{n+1/2}\right)\Delta y_k - \left(\tilde{\mathbf{G}}_k^{n+1/2}\right. \\
&\quad - s_{2k}\mathbf{W}_k^{n+1/2} - \frac{1}{Re}\tilde{\mathbf{S}}_k^{n+1/2}\right)\Delta x_k\Big],
\end{aligned}
$$

$$(4)$$

where $\Delta t = t^{n+1} - t^n$ is time step, $\mu_{i,j} = \int\int_{D_{i,j}} dx\,dy$ is volume of cell $D_{i,j}$, Δx and Δy are steps of the grid in x, y directions, vector $\mathbf{s}_k = (s_1, \ s_2)_k$ represents the speed of the edge k (see Fig. 2). The physical fluxes $\mathbf{F}$, $\mathbf{G}$, $\mathbf{R}$, $\mathbf{S}$ on the edge k of cell $D_{i,j}$ are replaced by the numerical fluxes (marked with tilde) $\tilde{\mathbf{F}}$, $\tilde{\mathbf{G}}$, $\tilde{\mathbf{R}}$, $\tilde{\mathbf{S}}$ which are approximations of the physical fluxes.
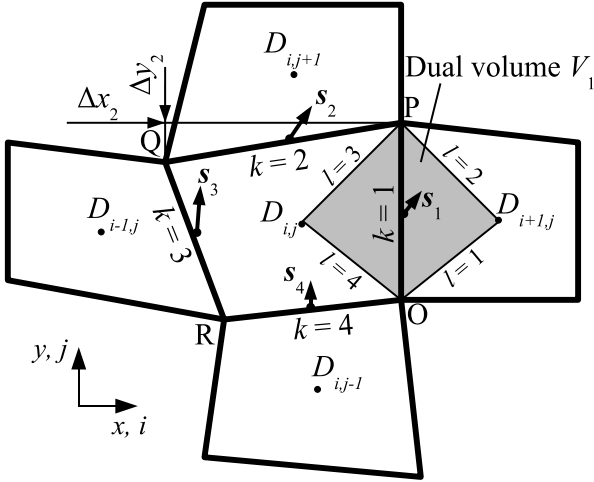
Figure 2: *Finite volume $D_{i,j}$ and the dual volume V_k'.*

The approximations of the convective terms $\mathbf{sW}_k$ and the numerical viscous fluxes $\tilde{\mathbf{R}}_k$, $\tilde{\mathbf{S}}_k$ on edge k are central. The higher partial derivatives of the velocity and the temperature in $\tilde{\mathbf{R}}_k$, $\tilde{\mathbf{S}}_k$ are approximated using dual volumes V_k' (see Fürst et al (2001)) as shown in Figure 2. The inviscid numerical fluxes are approximated by the physical fluxes from the cell on the left side of current edge in the predictor step and from the cell on the right side of current edge in the corrector step.

The last term used in MC scheme is the Jameson artificial dissipation (Jameson et al, 1981; Punčochářová et al, 2006):

$$AD(W_{i,j})^n = C_1\gamma_1\left(\mathbf{W}_{i+1,j}^n - 2\mathbf{W}_{i,j}^n + \mathbf{W}_{i-1,j}^n\right)$$
$$+C_2\gamma_2\left(\mathbf{W}_{i,j+1}^n - 2\mathbf{W}_{i,j}^n + \mathbf{W}_{i,j-1}^n\right), \quad (5)$$

$C_1, C_2 \in R$ are constants, in our case $C_1 = 1.7$, $C_2 = 1.5$ and the variables γ_1, γ_2 have the form:

$$\gamma_1 = \frac{|p_{i+1,j}^n - 2p_{i,j}^n + p_{i-1,j}^n|}{|p_{i+1,j}^n| + 2|p_{i,j}^n| + |p_{i-1,j}^n|},$$

$$\gamma_2 = \frac{|p_{i,j+1}^n - 2p_{i,j}^n + p_{i,j-1}^n|}{|p_{i,j+1}^n| + 2|p_{i,j}^n| + |p_{i,j-1}^n|}. \quad (6)$$

The term of artificial dissipation has the third order of accuracy then the second order of accuracy of the original scheme is valid. The vector of conservative variables $\mathbf{W}$ can be computed at a new time level t^{n+1}:

$$\mathbf{W}_{i,j}^{n+1} = \overline{\mathbf{W}}_{i,j}^{n+1} + AD(W_{i,j})^n. \quad (7)$$

The grid of the channels have successive refinement cells near the wall. The minimum cell size in y - direction is $\Delta y_{min} \approx 1/\sqrt{Re}$ to resolve capture boundary layer effects.

5. NUMERICAL RESULTS

The numerical results were obtained for the following input data: Mach number $M_\infty = 0.012$ ($u_\infty' = 4.116$ ms^{-1}), Re=5237, atmospheric pressure $p_2 = 1/\kappa$ ($p_2' = 102942$ Pa) at the outlet and frequencies of the wall oscillation f_A'=20 Hz and f_B'=100 Hz. The computational domain contained 450x50 cells.

The computation of the unsteady solution was carried out in two stages. Firstly the steady solution is realized, when channel between points A and B have rigid wall in the middle position of the gap. Then the steady solution is used as initial condition for the unsteady simulations.

Figure 3(a) shows the steady numerical solution which is the same initial condition for both unsteady solutions. The maximum of Mach number computed in the domain is $M_{max} = 0.173$ at $x = 2.317$ on the axis. Fig. 3(b) shows convergence to the steady state solution computed using the L_2 norm of momentum residuals (ρu). The convergence is satisfactory.
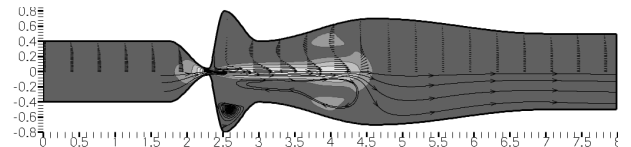
(a) $M_{max} = 0.173$ at $x = 2.317$, $g = 0.04$
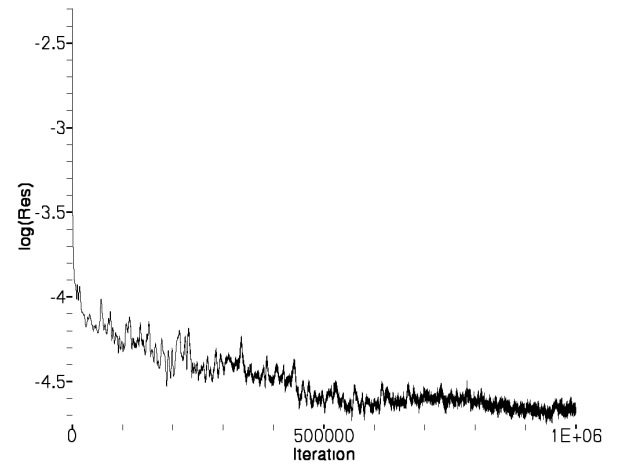
(b) Convergence to the steady state solution

Figure 3: *The steady numerical solution in D - $M_\infty = 0.012$, Re=5237, $p_2 = 1/\kappa$, 450x50 cells.*

5.1. Solution for frequency 20 Hz

The unsteady solution for frequency of the wall oscillation 20 Hz in the second period of the wall

oscillation is shown in Fig. 4 in several time layers. The highest Mach number $M_{max}' = 0.591$ was achieved in instant when the glottal width is opening just after the minimum of the gap is exceeded (in time $t = 2\pi + 0.609\pi$).
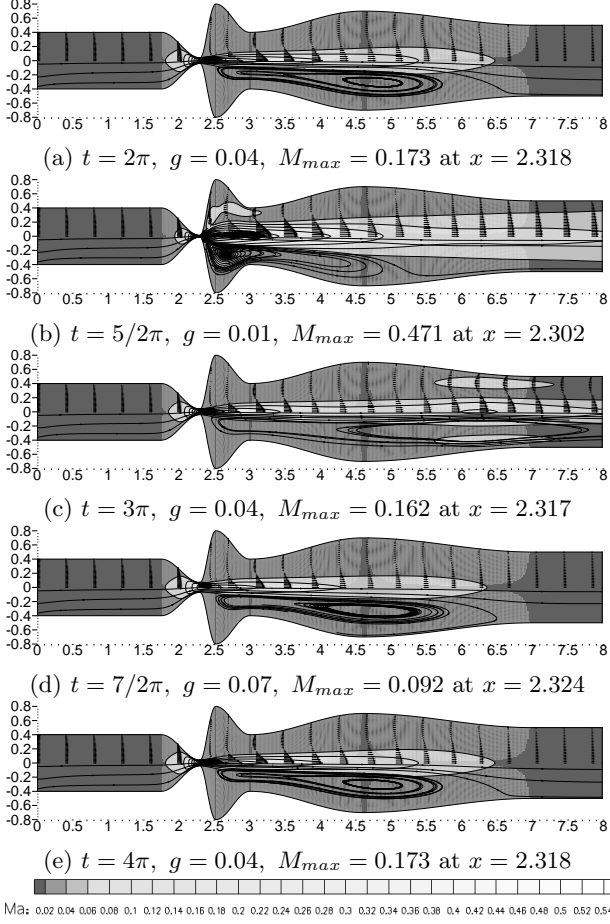

(a) $t = 2\pi$, $g = 0.04$, $M_{max} = 0.173$ at $x = 2.318$

(b) $t = 5/2\pi$, $g = 0.01$, $M_{max} = 0.471$ at $x = 2.302$

(c) $t = 3\pi$, $g = 0.04$, $M_{max} = 0.162$ at $x = 2.317$

(d) $t = 7/2\pi$, $g = 0.07$, $M_{max} = 0.092$ at $x = 2.324$

(e) $t = 4\pi$, $g = 0.04$, $M_{max} = 0.173$ at $x = 2.318$

Figure 4: *The unsteady numerical solution of airflow in D for wall oscillation - f_A'=20 Hz, $M_\infty = 0.012$, Re=5237, $p_2 = 1/\kappa$, 450x50 cells. Results are mapped by iso-lines of Mach number, by streamlines (lower part of the channel) and by velocity vectors (upper part of the channel).*

Figure 5 shows the changes of the gap g, Mach number and the pressure in real time at the distance x_C on the channel axis. The phase shifts between the minimum glottal gap g and the maximum of Mach number and pressure fluctuations are about 5.4×10^{-3} s and 2.9×10^{-3} s respectively. It can be also seen that the flow becomes periodical after the first period of the oscillations.

Figure 6 shows separation point area ratio A_s/A_{min} and flow rate at x_C over the second cycle. The area A_s denote separation area (the square of the width channel in separation point)
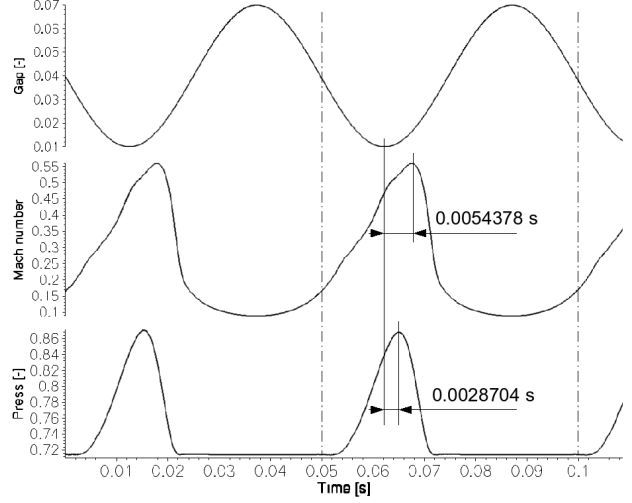

Figure 5: *Dimensionless gap g, Mach number and pressure at x_C on the channel axis in real time - $f_A' = 20$ Hz, $M_\infty = 0.012$, Re=5237, $p_2 = 1/\kappa$, 450x50 cells.*

and area A_{min} denote the square of the narrowest channel cross-section, i.e. the glottal width at x_C. The separation point is predicted to occur where the minimum pressure on the wall is achieved. The values of the ratio varied from $A_s/A_{min} = 1.005$, which occurred near the time of maximum gap, to $A_s/A_{min} = 16.99$ which occurred just after the gap opening phase starts.

5.2. Solution for frequency 100 Hz

The unsteady solution in the fourth period of the wall oscillation is shown in Fig. 7 in several time layers.

Figure 8 shows the Mach number along the axis of symmetry of the channel in several time instants during the oscillation period. Behind the narrowest channel cross-section ($x = x_C$) a second peak of the Mach number is forming which travels as a dying wave to the outlet. The highest Mach number $M_{max} = 0.557$ was achieved in the instant when the glottal width is opening just after the minimum of the gap is exceeded in time $t = 6\pi + 0.84\pi$.

Figure 9 shows the changes of the gap g, Mach number and the pressure in real time at the distance x_C on the channel axis. The phase shifts between the minimum glottal gap g and the maximum of Mach number and pressure fluctuations are about 1.7×10^{-3} s and 7.8×10^{-4} s respectively. It can be also seen that the flow becomes
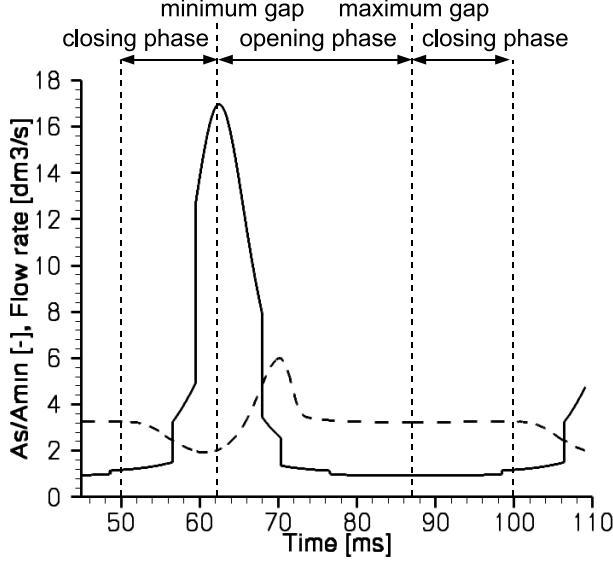
Figure 6: *Separation point area ratio (solid line) and flow rate (dashed line) at x_C over the second cycle - $f'_A = 20$ Hz, $M_\infty = 0.012$, Re=5237, $p_2 = 1/\kappa$, 450x50 cells.*

periodical after the first period of the oscillations.

Figure 10 shows separation point area ratio A_s/A_{min} and flow rate at x_C over the fourth cycle. The values of the ratio varied from $A_s/A_{min} = 1.003$, which occurred near the time of maximum gap, to $A_s/A_{min} = 6.209$ which occurred just after gap opening.

6. DISCUSSION AND CONCLUSION

The special program code has been developed for solving the 2D unsteady Navier-Stokes equations for compressible fluid and used for the numerical simulation of the airflow in the glottal region.

Due to a lack of experimental data, the results can be partially compared with the article by Decker and Thomson (2007). They computed flow separation point and glottal flow rate in a geometrically different channel for the vibration frequency 447 Hz using FE model of the vocal folds and incompressible Navier-Stokes equations. They found that the separation area ratio was in the range $A_s/A_{min} = 1.3 - 9.7$ corresponding to our results, the maximum flow rate and maximum glottal width were in phase and the minimum pressure lagged by approximately 1/10 of one period. This does not correspond to our findings, where the maximum flow rate and pressure are delayed related to the minimum gap.
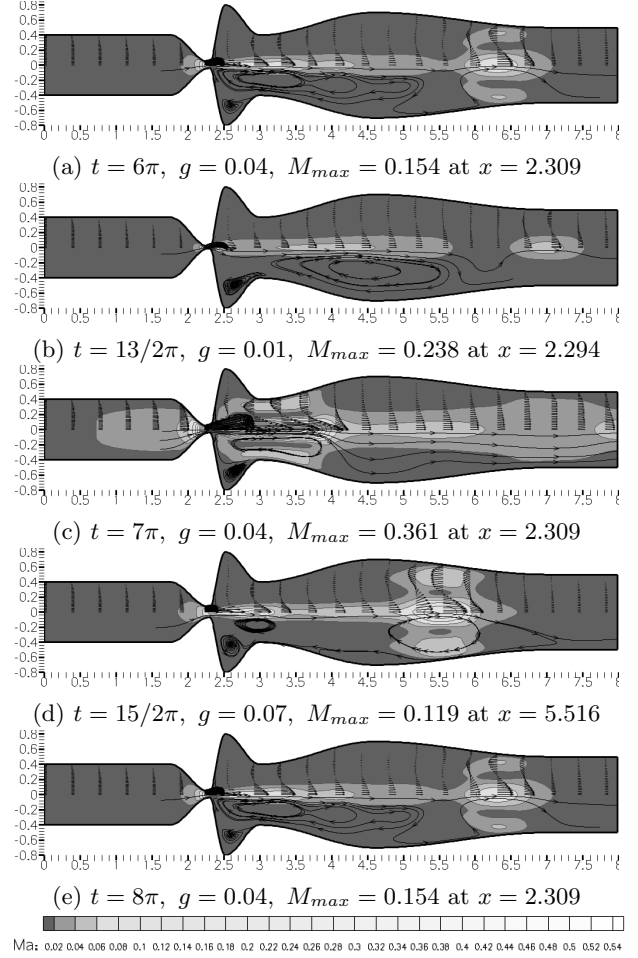

(a) $t = 6\pi$, $g = 0.04$, $M_{max} = 0.154$ at $x = 2.309$

(b) $t = 13/2\pi$, $g = 0.01$, $M_{max} = 0.238$ at $x = 2.294$

(c) $t = 7\pi$, $g = 0.04$, $M_{max} = 0.361$ at $x = 2.309$

(d) $t = 15/2\pi$, $g = 0.07$, $M_{max} = 0.119$ at $x = 5.516$

(e) $t = 8\pi$, $g = 0.04$, $M_{max} = 0.154$ at $x = 2.309$

Figure 7: *The unsteady numerical solution of airflow in D for wall oscillation - f_B'=100 Hz, $M_\infty = 0.012$, Re=5237, $p_2 = 1/\kappa$, 450x50 cells. Results are mapped by iso-lines of Mach number, by streamlines (lower part of the channel) and by velocity vectors (upper part of the channel).*

It could be caused by consideration of fluid compressibility in our study.

A higher maximum flow rate was obtained for higher frequency. From the position of sudden jumps in the ratio A_s/A_{min} in the opening and closing phases (see Figs. 6 and 10) it can be deduced that the flow separation point is shifted stream wise in closing phase comparing to the glottis opening phase.
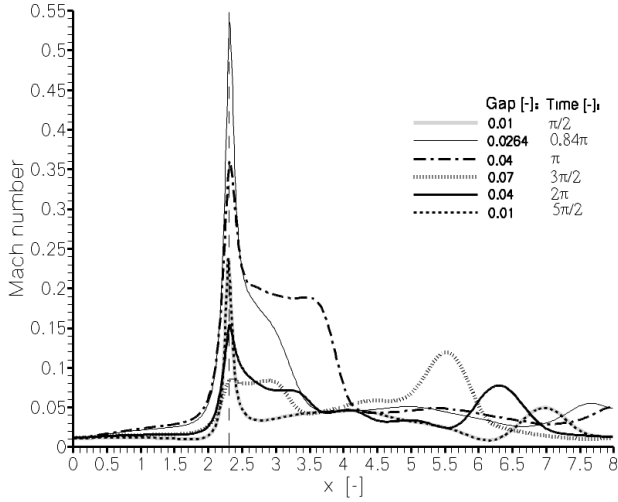
7. ACKNOWLEDGEMENT

Figure 8: *Mach number along the channel axis in several time instants. Data computed during the fourth oscillation period-* $f'_B = 100$ *Hz,* $M_\infty = 0.012$, *Re=5237,* $p_2 = 1/\kappa$, *450x50 cells.*

8. REFERENCES

Fürst, J., Janda, M., Kozel, K., 2001 Finite volume solution of 2D and 3D Euler and Navier-Stokes equations. In *Mathematical fluid mechanics* (eds. Neustupa, J. & Penel, P.), 173-194. Berlin.

Honzátko, R., Horáček, J., Kozel, K., 2006, Solution of inviscid incompressible flow over a vibrating profile. *COE Lecture notes* **3**: 26-32. (eds M. Beneš & M. Kimura & T. Nataki), Kyushu university. ISSN 1881-4042.

Jameson, A., Schmidt, W., Turkel, E., 1981, Numerical solution of the Euler equations by the finite volume methods using Runge-Kutta time-stepping schemes. *AIAA*, 81-125.

Punčochářová, P. and Kozel, K. and Fürst, J., 2006, An unsteady numerical solution of viscous compressible flows in a channel. In *Program and Algorithms of Numerical Mathematics 13*, Math. Institute ASCR, 220-228. ISBN 80-85823-54-3.

Decker, G.Z., Thomson, S.L., 2007, Computational simulations of vocal folds vibration: Bernoulli versus Navier-Stokes. *Journal of Voice*, **21**(3): 273-284.
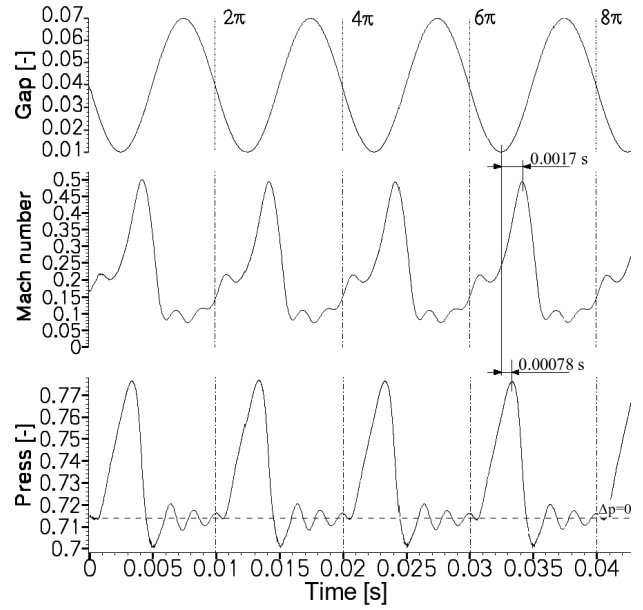
Figure 9: *Dimensionless gap g, Mach number and pressure at* x_C *on the channel axis in real time. Data computed during the fourth oscillation period-* $f'_B = 100$ *Hz,* $M_\infty = 0.012$, *Re=5237,* $p_2 = 1/\kappa$, *450x50 cells.*
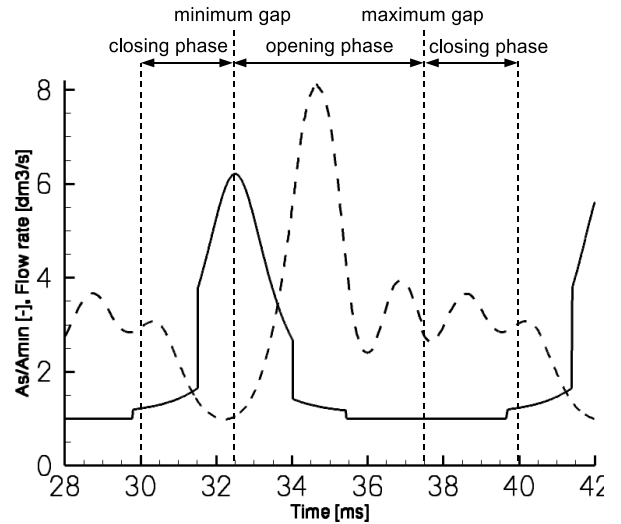

Figure 10: *Separation point area ratio (solid line) and flow rate (dashed line) at* x_C *over the fourth cycle -* $f'_B = 100$ *Hz,* $M_\infty = 0.012$, *Re=5237,* $p_2 = 1/\kappa$, *450x50 cells.*